Development of an Agent-Based Model for the Secondary Threat Resulting from a Ballistic Impact Event

Matthew J. Bova
Department of Mathematical Sciences
University of Cincinnati
Cincinnati, Ohio 45221 USA

Frank W. Ciarallo
Department of Biomedical, Industrial & Human Factors Engineering
Wright State University
Dayton, Ohio 45435 USA

Raymond R. Hill
Department of Operational Sciences
Air Force Institute of Technology
Wright-Patterson AFB, Ohio 45433 USA

Abstract

The process by which a high-velocity impact event leads to fire ignition onboard military vehicles is complex, influenced by the interaction of heated debris fragments and fuel spurting from ruptured tanks. An assessment of the risk of such a fire begins with a complete characterization of the secondary threat resulting from the impact, including debris fragment sizes, states of motion, and thermal properties. In the aircraft survivability community, there is a need for an analytical tool to model this complete threat. This paper approaches the problem by proposing an agent-based simulation model of the fragments in a debris cloud. An analytical/empirical impact fragmentation model is developed for incorporation into the simulation model, which determines fragment sizes and states of motion. Future work focuses on an agent-based approach to modeling the thermal profile of the threat, treating each fragment in the cloud as an individually (though not autonomously) cooling "lump" of uniform temperature. Development and study of this proof-of-concept effort leads to a deeper understanding of such secondary threats and demonstrates the value of agent-based simulation models as analytical tools.

Keywords
Defence studies; agent-based modeling; ballistic impacts; survivability

Introduction and Background

Developing a complete characterization of the secondary threat resulting from a high-velocity projectile impact on the exterior of an aircraft body is of particular concern to the aircraft survivability community. Such ballistic impacts typically result in penetration of the body, generating clouds of debris fragments and releasing large quantities of thermal energy. The

potential threat of the resulting debris cloud and its thermal profile is magnified if the impact occurs in areas near a source of fuel. In such cases, the prevention of potential onboard fires is of utmost concern to vulnerability analysts.

Figure 1, from Bestard and Kocher (2010), depicts a ballistic impact event. The second frame shows the point of impact, where the deformation of the impactor (a fragment from a proximity missile) and its target occurs. This typically results in an observable "flash" of radiant thermal energy on the impact-side of the target. The third frame shows the resulting debris cloud and a second exit-side flash moving away from the target. A complete description of this secondary threat requires integrated models for the evolution of both the debris cloud and its thermal properties as functions of time.

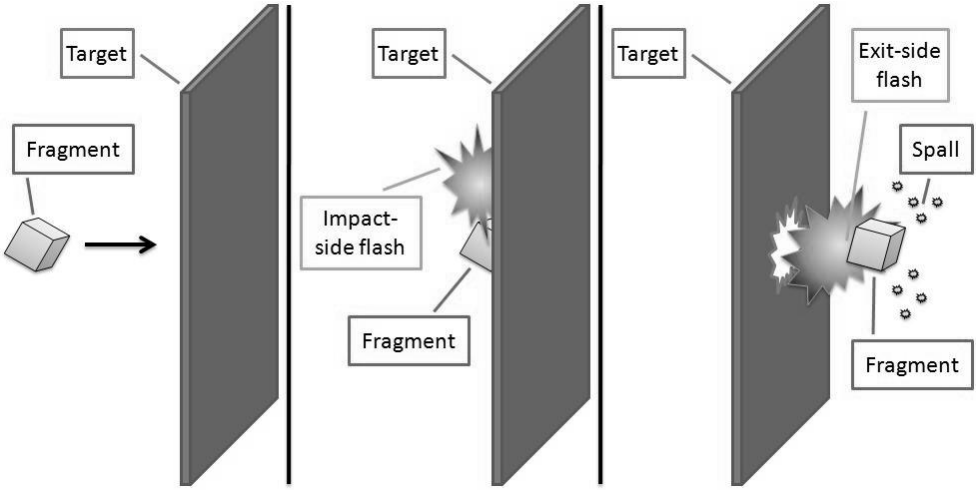

Figure 1 Depiction of a ballistic impact event.

There have been numerous approaches to the task of modeling the fragmentation induced by a high-velocity impact and the evolution of the resulting debris cloud. Most of these efforts focus on predicting the damage to "secondary targets", such as an aircraft's internal fuel bladders, when impacted by debris clouds formed from the initial impact event. One such approach is the engineering model discussed in Yatteau and Dickinson (1993) for the prediction of central hole damage to metallic "witness" plates behind the initial target. This model has been included in the much larger FATEPEN (Fast Air Target Encounter Penetration) model, a set of computer codes developed for the Naval Surface Warfare Center and used in system vulnerability assessments (Yatteau, 1982). Schonberg (1995) provides a comparison of FATEPEN to similar models,

notably PEN4 (Bjorkman *et al*, 1987), KAPP (Snow, 1992), and KAPP-II (Greer and Hatz, 1992).

Schäfer (2006) offers a different approach to the modeling of post-impact debris, noting that models such as FATEPEN, PEN4, and KAPP/KAPP-II have not considered rigorous consistency with physics-based laws related to the conservation of mass, momentum, and energy. The Schäfer engineering fragmentation model utilizes the conservation laws to allow a fully integrated approach to motion-based and energy-based relationships. To allow this, the model starts with assumptions regarding the shape of the debris cloud, leading to an integrated system of equations describing the system. In support of this approach, other works worthy of mention are the physics-based approaches discussed in Kipp *et al* (1993) and Grady and Winfree (2001).

Some studies at the Air Force Institute of Technology (AFIT) have focused solely on the development of a thermal model for a ballistic impact event. A particular effort discussed in Talafuse *et al* (2011) models the boundary of the luminous flash regions produced by such impacts. This approach centers on fitting ellipses to the flash area presented on high-speed video, measuring the ellipse and using these measures to build a predictive boundary model of the flash via regression analysis. The high-speed video data was collected by the Aerospace Survivability and Safety Operating Location (96 TG/OL-AC) at Wright-Patterson Air Force Base (WPAFB). Bestard and Kocher (2010) discusses the collection of this video data as well as the methodology used to quantify it.

A parallel effort discussed in Pyles and Disimile (2011) proposes a physics-based model for the thermal profile of a ballistic impact flash. This approach focuses on several mechanisms leading to the flash in order to predict the heat released in the flash as a function of time. Integration with the boundary models formulated at AFIT leads to a complete empirically-based thermal model.

Despite these efforts to model high-velocity impacts, few adequate analytical tools exist that model the complete secondary threat of the debris cloud and its thermal properties. There is a clear need for such a tool that can be incorporated into vulnerability assessments to help evaluate the risk of fire ignition onboard military vehicles. Unfortunately, the dynamic aspects of high-velocity impacts, and the resulting flashes, all but rule out an analytical modeling approach. The chaotic nature of such impact events has led to our choice of an agent-based model to describe the system. The benefit of the agent-based approach stems from the ability to model complex

system behaviors using comparatively simple agent rules and multi-agent interactions (Heath and Hill, 2010). The present work represents an extension of an initial proof-of-concept effort discussed in Bova *et al* (2013). In particular, this paper discusses the development of an analytical/empirical impact fragmentation model and its incorporation into an agent-based simulation model of ballistic impact events. An initial evaluation of the adequacy of the fragmentation model is made by comparing simulation model output to empirical findings from the literature. Finally, a notional agent-based approach to modeling the thermal profile of a ballistic impact is proposed, which is the center of future work.

Simulation Model Development

The ballistic impact simulation model (BISM) was built using AnyLogic multi-method modeling software. The model focuses on the specific case of a mild steel cubic impactor (representative of threats from a detonated proximity missile) striking an aluminum alloy target panel (representative of an aircraft body). For this type of impact, live fire panel testing data was obtained from the 96 TG/OL-AC at WPAFB and used in model development. O'Connell *et al* (2010) discusses the detailed testing plan for this series of live fire shots. The range of impact conditions analyzed consists of the following:

- Impactor size – 20, 40, 75, and 150 grains;
- Intended impact velocity – 4000 and 7000 ft/sec;
- Target panel material – aluminum 2024 and aluminum 7075;
- Target panel thickness – 0.063, 0.09, 0.16, and 0.25 in; and
- Impact obliquity angle – 0 and 45 degrees.

Note that the obliquity angle refers to the angle between the flight path of the impactor and the normal-to-the-surface of the target panel at the point of impact. These independent variables (threat size, impact velocity, target material, target thickness, and obliquity) serve as the inputs to the simulation model. However, currently only impacts at normal incidence (0 degree obliquity) are considered.

Figure 2 provides a flowchart of the general model logic. The user inputs the impact conditions, specifying the impactor and target properties and the impact velocity, V_i. Based on

these inputs, the model determines whether the impact results in perforation of the target or ricochet. This determination is based upon the ballistic limit velocity for the impact conditions, V_{50}, calculated using the formula recommended by the Joint Technical Coordinating Group for Munitions Effectiveness (1985). The JTCG/ME's approach to calculating V_{50} involves a preliminary calculation of the presented area of the threat on impact. For a cube-shaped impactor the presented area, A_{pr}, (in m^2) is calculated as

$$A_{pr} = 1.50 {l_i}^2, \tag{1}$$

where l_i is the length of the impactor in meters. Denoting m_i as impactor mass (in kg), ρ_i as impactor density (in kg/m^3), T_p as target panel thickness (in m), and θ as the obliquity angle, V_{50} (in m/sec) is then

$$V_{50} = C_{bf} \left(\frac{\rho_i T_p A_{pr}}{m_i}\right)^{b_f} sec^h\theta \left(\frac{\rho_i T_p A_{pr}}{m_o}\right)^{f} = C_{bf}\ {Q_8}^{b_f}\ sec^h\theta\ {Q_{11}}^{f}, \tag{2}$$

where C_{bf}, b_f, h, m_o, and f are constants based on the physical properties of the impacting materials (mild steel and aluminum).

For $V_i \leq V_{50}$, the impactor ricochets off the target panel. In this case the simulation ends and a ricochet is recorded as the result of the run. For $V_i > V_{50}$, the impactor perforates and completely penetrates the panel. The model generates the populations of fragments (from both the impactor and the target) that form the resulting debris cloud. Each fragment is modeled as an agent, with an assigned type, size, and initial state of motion. The "time zero" computations end with a calculation of the initial kinetic energy of the debris cloud.

At each time step, the position of each fragment in the debris cloud is updated. If a fragment has reached a rear wall 12 inches (300 mm) behind the initial target, it is stopped. As time advances in the simulation, the position of each fragment agent in the debris cloud evolves according to the physical laws of motion. Once all fragments have reached the rear wall, the simulation ends and the output data is recorded for the run.

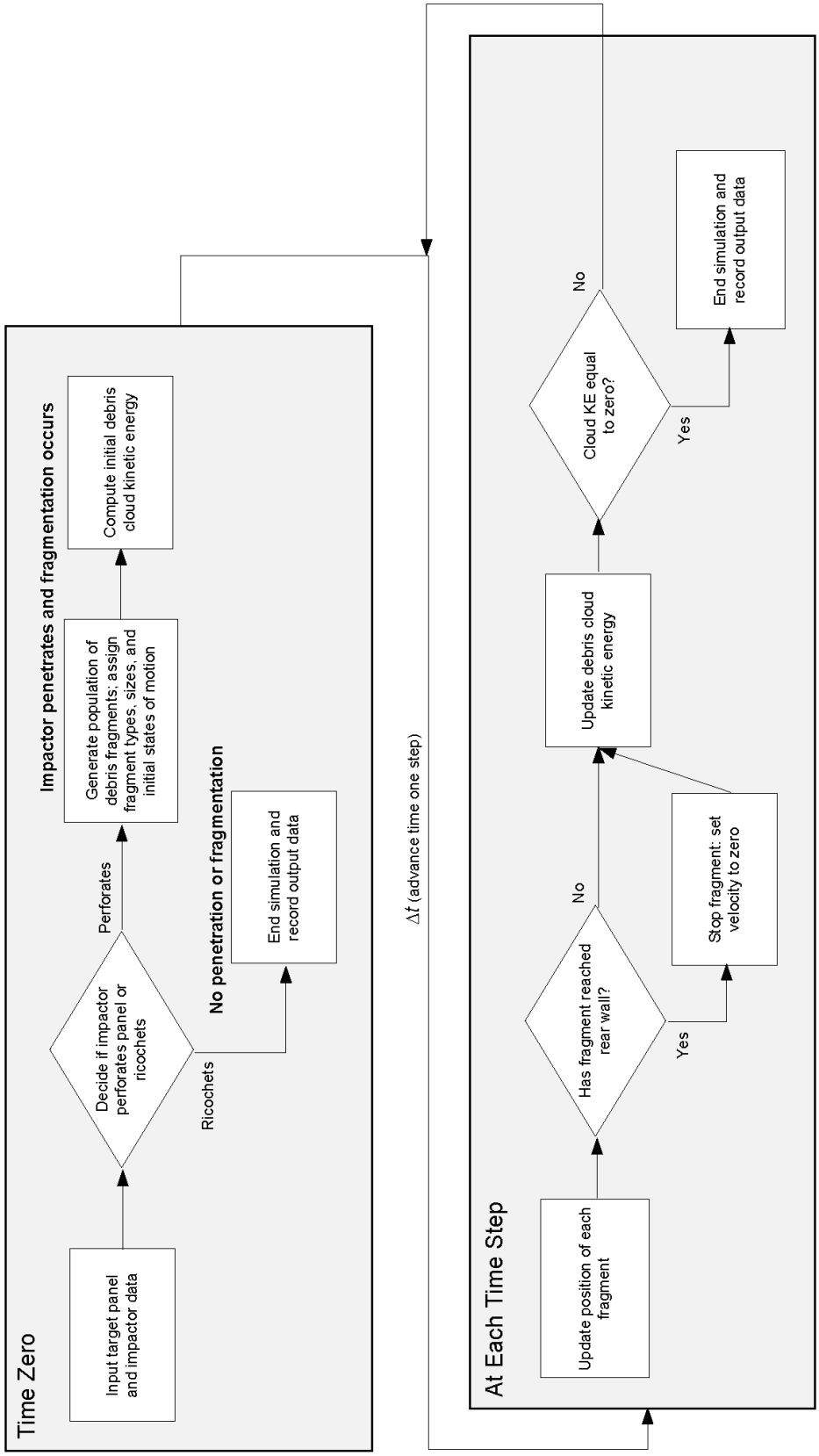

Figure 2 Flowchart of the BISM logic.

An analytical/empirical impact fragmentation model drives the generation of the debris fragments during a simulation run, including the assignment of fragment types, sizes, and initial states of motion. This model, developed specifically for incorporation into BISM, consists of three components: partitioning of the post-impact mass into fragment quantities and their associated mass, determination of a distribution for fragment sizes, and construction of the initial shape and state of motion of the debris cloud. The development of these components is the subject of the following sub-sections.

Partitioning of Post-Impact Mass

It is assumed that only exit-side debris is created by the impact, resulting in an over-estimate of the mass and momentum in the cloud. This is based on live fire experiments for the impact of hardened steel spheres on mild steel targets discussed in Yatteau and Dickinson (1993). In these tests, 80-90% of the total system mass (the sphere and the material removed from the target) was accounted for on the exit-side of the impact.

As in Schäfer (2006), the total number of fragments, N, present in a debris cloud is partitioned as follows

$$N = 1 + N_s + N_p \,, \tag{3}$$

where N_s represents the number of spall fragments from the impactor and N_p represents the number of fragments from the target panel. The additional fragment in Eq. (3) accounts for the residual portion of the penetrating impactor. Conservation of mass requires

$$m_i = m_{ri} + \sum_{j}^{N_s} m_{s,j} = m_{ri} + M_s \quad \text{and} \quad M_p = \sum_{k}^{N_p} m_{p,k} \,, \tag{4}$$

where m_i is impactor mass, m_{ri} is impactor residual mass (post-impact), $m_{s,\,j}$ is the mass of the jth spall fragment, M_s is the total mass of the spall fragments, $m_{p,\,k}$ is the mass of the kth target panel fragment, and M_p is the total mass of the target panel fragments. Conservation of momentum is represented as in Grady and Winfree (2001):

$$m_i V_i = (m_{ri} + M_s + M_p) V_r \,, \tag{5}$$

where V_i is the impact velocity and V_r is the residual velocity of the mass-center of the debris cloud. Utilizing Eqs. (4) and (5), the total masses of the spall and panel fragments are

$$M_s = m_i - m_{ri} \,, \tag{6}$$

$$M_p = m_i \frac{V_i}{V_r} - (m_{ri} + M_s) = m_i \frac{V_i}{V_r} - m_i \,. \tag{7}$$

Now m_i and V_i are model inputs and known. Thus, to solve for M_s and M_p, we need only determine m_{ri} and V_r. For this task, we take an empirical approach and utilize the live fire test data obtained from the 96 TG/OL-AC. In the data, observed values of m_{ri} and V_r are recorded for each shot. We perform a regression analysis on these observations, developing models for these variables for each target panel material (a total of 4 models).

In the regression models for m_{ri}, the residual weight of the impactor, w_{ri}, is used as the dependent variable (note that $m = w/g$, where g is standard acceleration due to gravity). This is done to utilize the formula for residual weight recommended by JTCG/ME (1985) as a predictor in the model:

$$w_{ri,d} = w_i - w_i C_m \left(\frac{\rho_i T_p A_{pr}}{m_i}\right)^q \left(\frac{V_i}{c_1}\right)^v \left(\frac{\rho_i T_p A_{pr}}{m_o}\right)^t sec^s = w_i - w_i C_m {Q_8}^q {Q_{10}}^v {Q_{11}}^t sec^s\theta \,, \tag{8}$$

where $w_{ri,d}$ is the predicted residual weight of a mild steel cubic impactor of weight w_i undergoing "deformation-mode" mass loss. As in Eq. (2), C_m, q, c_1, v, m_o, t and s are constant values based on the impacting materials and θ is the obliquity angle. The selected "best" specification for the w_{ri} models (for both the 2024 and 7075 panel materials) is as follows

$$w_{ri} = \beta_o + \beta_1 w_{ri,d} + \beta_2 w_i {V_i}^2 + \beta_3 \theta l_i + \varepsilon \,, \tag{9}$$

where l_i is the length of the impactor. A summary of the model for aluminum 2024 is provided in Table 1.

Table 1 The w_{ri} Model for Aluminum 2024 (R^2 = 0.7656)

Term	*Coeff. Est.*	*Std. Error*	*t-value*	*p-value*	*VIF*
Intercept	2.308e-03	1.949e-03	1.184	0.238	-
$w_{ri,\,d}$	9.441e-01	4.903e-02	19.256	< 2e-16	1.490
$w_i V_i^2$	-7.251e-08	9.229e-09	-7.857	1.00e-12	1.490
θl_i	3.536e-02	5.486e-03	6.446	1.79e-09	1.040

The selected "best" specification for the V_r regression models (for both the 2024 and 7075 panel materials) contains only two predictors, V_i and the calculated ballistic limit velocity V_{50}:

$$V_r = \beta_o + \beta_1 V_i + \beta_2 V_{50} + \varepsilon\,. \tag{10}$$

This specification is less complicated than the w_{ri} model, yet produces R^2 values exceeding 0.98 for both panel materials. A summary of the model for aluminum 2024 is provided in Table 2.

Table 2 The V_r Model for Aluminum 2024 (R^2 = 0.9839)

Term	*Coeff. Est.*	*Std. Error*	*t-value*	*p-value*	*VIF*
Intercept	134.67919	16.782356	8.025	2.63e-13	-
V_i	0.897846	0.009532	94.194	< 2e-16	1.038
V_{50}	-0.77873	0.021377	-36.428	< 2e-16	1.038

Utilizing these regression models, M_s and M_p can be determined in Eqs. (6) and (7), thus fully specifying the partitioning of fragment quantity and mass within the debris cloud. When implementing the four regressions into the BISM code, a normally-distributed error term is added to each model with a mean of 0 and variance based on the variance of the residuals.

Distribution of Debris Fragment Sizes

Each fragment in the debris cloud is modeled as a spherical object. The diameter of the residual impactor is determined from its computed residual mass m_{ri} and its material density (approximately 7850 kg/m^3 for mild steel). The residual impactor is generated at time zero in the simulation and assigned these properties. The generation of the spall and panel fragments at time

zero depends on their total masses, M_s and M_p, and a distribution for their sizes. For these sizes, we employ an exponential distribution for mass *m* similar to that used in Schäfer (2006):

$$F(m) = 1 - \exp\left(-\frac{m}{m_{a,j}}\right), \tag{11}$$

where *F(m)* is the cumulative distribution function of mass *m*, $m_{a,j}$ is the average fragment mass, and *j* = *s*, *p*. Eq. (11) is a simplified form of the Rosin-Rammler (Weibull) distribution discussed in Grady and Winfree (2001):

$$F(x) = 1 - \exp[-(x/\sigma)^n], \tag{12}$$

where *x* is the fragment characteristic size and σ is the fragment size scale. The parameter *n* is typically near 1.

In Schäfer (2006), Eq. (11) is used to describe the masses of spall fragments generated from the impact of aluminum spheres on thin aluminum target panels at hypervelocity. However, the Rosin-Rammler form is a popular empirical distribution used to describe fragment sizes resulting from several different fragmentation processes, not just the dynamic fragmentation process of a high-velocity impact event (Grady and Kipp, 1985). Due to both its simple form and popularity, this distribution is selected for use in the current BISM prototype.

To implement Eq. (11), the average fragment mass $m_{a,j}$ is needed for both the population of spall fragments and the population of panel fragments. To determine $m_{a,j}$, the average fragment diameter is computed and then the material density of the spherically-modeled fragments (mild steel or aluminum) is used. Kipp *et al* (1993) provides a method for calculating the average diameter of spherical fragments based on three modes of failure: (1) facture toughness dominated failure, (2) yield strength dominated failure, and (3) surface tension dominated failure. In the current iteration of the model, we consider only the first mode of failure, for which average diameter $d_{a,j}$ (in meters) is

$$d_{a,j} = \left(\frac{\sqrt{24} \times K_{c,j}}{\rho_j \times c_j \times \varepsilon_{sr}}\right)^{2/3}, \tag{13}$$

where $K_{c,\,j}$ is plane strain fracture toughness (Pa $m^{1/2}$), ρ_j is material density (kg/m^3), c_j is bulk sound velocity (m/sec), ε_{sr} is average strain rate (1/sec), and $j = s, p$.

In determining the average strain rate, we follow the approach used in Schäfer (2006) by first calculating the "maximum engineering strain rate,"

$$\varepsilon_{sr,max} = V_i / l_i \,, \tag{14}$$

where V_i is impact velocity in m/sec and l_i is impactor length in meters. This is a measure of the maximum strain rate the impactor and target panel experience during the impact event. In Schäfer (2006), a fit factor $f_\varepsilon = 0.3$ is then introduced to Eq. (14) in order to fit the strain rate calculation to experimental data. However, the live fire data obtained from the 96 TG/OL-AC for model development does not contain information on debris fragment quantities or sizes. Without experimental data, we currently employ a notional fit factor of 0.4. Thus,

$$\varepsilon_{sr} = f_\varepsilon \varepsilon_{sr,max} = 0.4 \varepsilon_{sr,max} \,. \tag{15}$$

As a result of Eqs. (13) – (15), $d_{a,\,j}$ decreases as V_i increases (holding all else fixed) and increases as l_i increases (holding all else fixed). For the impactor sizes (20, 40, 75, and 150 grains), impact velocities (4000, 7000 ft/sec), and target materials (2024, 7075) considered, we obtain the ranges for average fragment diameter shown in Table 3. Validation of these ranges, as well as the choice of f_ε, awaits the availability of necessary experimental data.

Table 3 Ranges for Debris Fragment Average Diameters (in mm)

Target Panel	*Impactor Spall Fragments*	*Panel Fragments*
2024	1.2 - 3.3	1.8 - 5.0
7075	1.2 - 3.3	1.2 - 3.3

The flowchart in Figure 3 illustrates the logic for spall and panel fragment generation in BISM, utilizing Eq. (11) for the fragment size distribution. The algorithm begins by initializing M_j, the total mass of the population of fragments ($j = s, p$). A debris fragment is then created and assigned a draw from Eq. (11) for its mass. An initial check is then made to see if subtracting the

fragment's mass from M_j will result in a negative value. If so, the fragment is re-assigned a draw from Eq. (11). Once the fragment is assigned an "acceptable" mass, M_j is decremented by that amount of mass. The creation of fragments continues until M_j falls below $m_{a,\,j}$, the average fragment mass. Thus, a small amount of unused mass (between 0 and $m_{a,\,j}$) is always leftover. This is purposely done to reduce the over-estimation of exit-side mass in the debris cloud (since only exit-side debris is assumed to be created by the impact, which does not hold in reality).

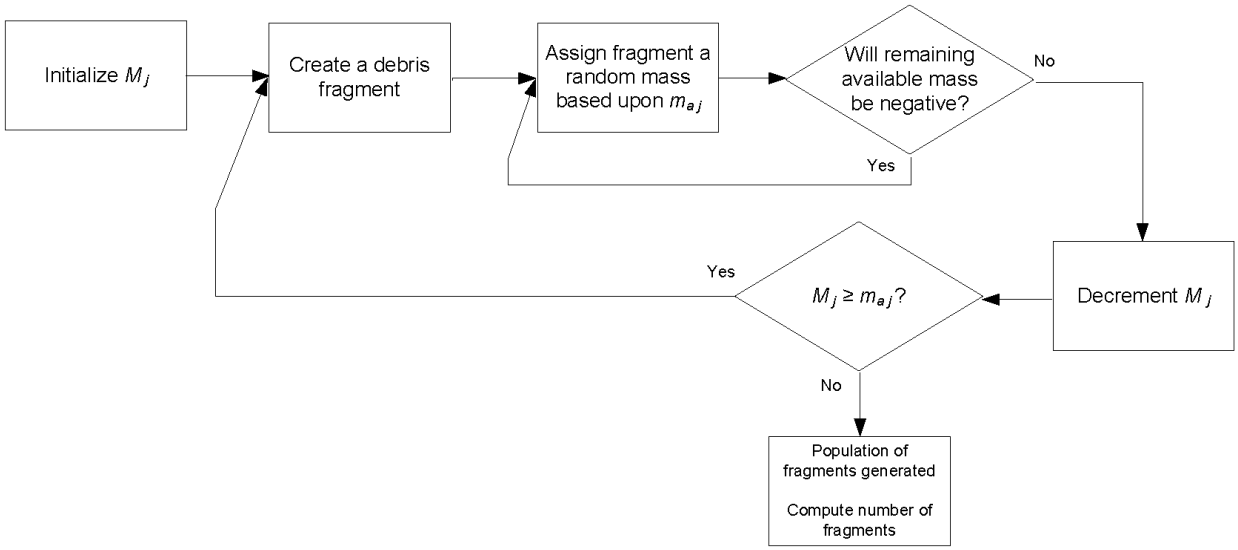

Figure 3 Flowchart of the logic for impactor spall and panel fragment generation in BISM.

Initial Debris Cloud Shape and State of Motion

Time zero in the simulation model is assumed to be immediately after the impactor completely penetrates the target panel. At this instance in time, it is assumed that all fragments in the debris cloud initially lie within a section of a spherical shell, illustrated in Figure 4. This initial shape is chosen based upon Schäfer (2006), where it is assumed that the impactor spall and panel fragments generated from a hypervelocity impact are distributed evenly on the surfaces of expanding spherical and ellipsoidal shells, respectively. This characterization of the debris cloud is made at some instance in time after impact where the fragments have already begun to move outward from the point of impact. Since our focus lies in describing a debris cloud at its inception (and generated from much slower impact velocities), we use a section of a spherical shell as a reasonable approximation for the initial bounding region.

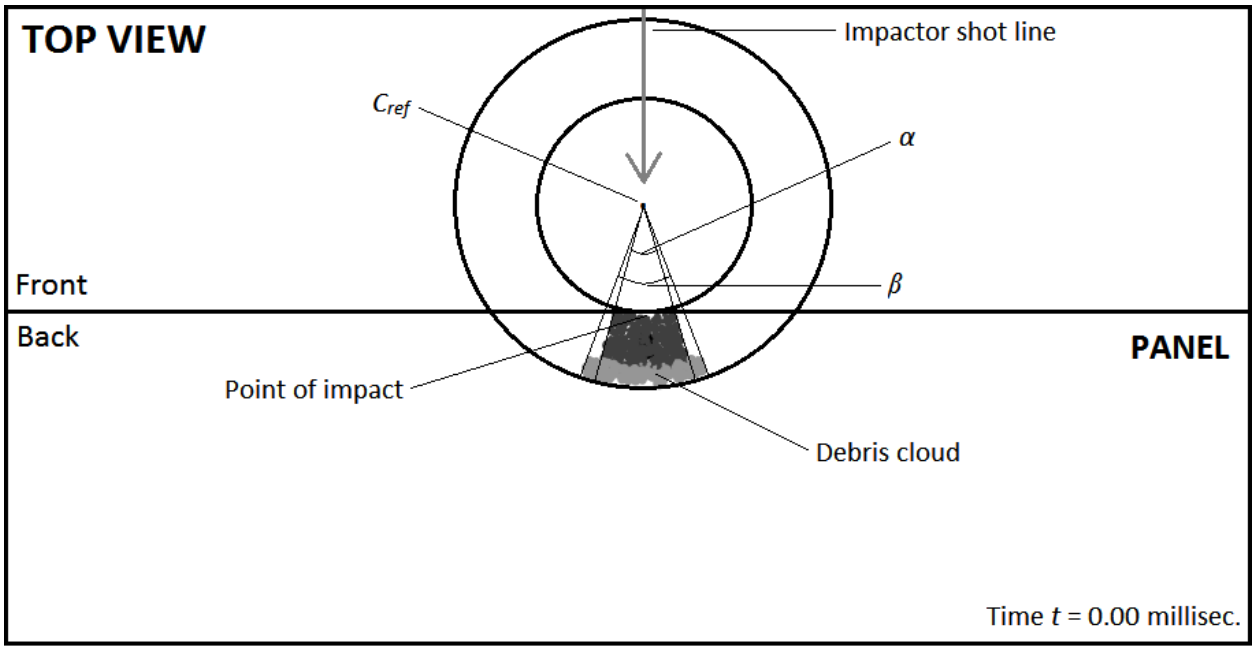

Figure 4 Screenshot of BISM's 2D "top view" animation window at simulated time zero, showing the debris fragments lying within a section of the outlined spherical shell. The panel fragments (light gray) lie in front of the residual impactor and its spall fragments (dark gray).

To create this initial region, it is first assumed that the projected area of an approximately square hole in the target panel is equal to A_{pr}, the presented area of the impactor calculated in Eq. (1). The radial width of the spherical shell section, r_{dc}, is then set approximately equal to $1.25l_i$, where l_i is impactor length (pre-impact). Letting α denote the spread angle of spall fragments (the panel fragments are assigned a spread angle of β), we have the following equation for d_{ref}, the distance from the point of impact to a point C_{ref} along the impactor shot line (see Figure 4):

$$d_{ref} = \frac{\sqrt{A_p} + 2\, r_{dc} \sin\alpha}{2 \sin\alpha} - r_{dc}. \tag{16}$$

The residual portion of the impactor is initially located on the exit-side of the panel along the shot line. Each spall fragment is located around the residual impactor independent of mass based on a set of uniformly-drawn spherical coordinates (r, γ, φ), where r is the radial distance from C_{ref}, γ is the azimuth angle, and φ is the inclination angle. As shown in Figure 4, the spall fragments (dark gray) reside behind the panel fragments (light gray) within a region defined by

$-\alpha \leq \gamma \leq \alpha$, $-\alpha \leq \varphi \leq \alpha$. Each panel fragment is also given uniformly-drawn spherical coordinates independent of mass which place it around the residual impactor and spall fragments within a region defined by $-\beta \leq \gamma \leq \beta$, $-\beta \leq \varphi \leq \beta$.

The initial resultant velocity of each fragment in the debris cloud is set equal to V_r, the residual velocity of the mass-center of the cloud determined via the regression model specified in Eq. (10). The trajectory of the residual impactor is assumed to be unchanged so that it continues to travel along its shot line. However, each impactor spall and panel fragment's initial direction is stochastically determined. Denoting $\gamma_{xy,f}$ as the initial azimuth direction angle and $\varphi_{yz,f}$ as the initial inclination direction angle of fragment *f*, its initial trajectory is assigned to be

$$\begin{cases} \gamma_{xy,f} = \gamma_f + \tau_f \\ \varphi_{yz,f} = \varphi_f + \tau_f \end{cases}, \tag{17}$$

where γ_f and φ_f are the angular coordinates determining fragment *f*'s initial location in the cloud and τ_f is a stochastic error term.

This error term is included to capture some of the chaotic nature of a ballistic impact event, due to the fact that trajectories of the resulting debris are not easily definable using deterministic methods. However, using stochastic initial trajectories present a possible issue in the simulation model: fragments may collide with each other as the debris cloud evolves over time. In reality, such collisions are not likely to happen after impact fragmentation has occurred and the debris has been set in motion. To resolve this issue, all collisions between fragments are treated as perfectly elastic in BISM. At each time step in the simulation, fragments search for adjacent neighbors and resolve any collisions as part of the update of their position (see Figure 2). Kinetic energy and momentum are conserved in these collisions.

The spread angles α and β and the error term τ_f must be fit variables in the model since they determine the initial spread and overall spray angle of the debris cloud. Without the necessary experimental data to determine a suitable range for these variables, we select notional values for now. In the current BISM prototype, α and β are set to 15 and 20 degrees, respectively, so that the panel fragments have a wider spread angle. The error term τ_f is distributed uniformly between -5 and 5 degrees, with an independent draw for each impactor spall and panel fragment. These values are selected in an attempt to match the morphology assumptions made in Schäfer (2006) for a later stage of debris cloud evolution.

Initial Evaluation of the Fragmentation Model

With validation of the impact fragmentation model awaiting necessary experimental data, we conduct a simulation experiment as an initial assessment of the model's performance and adequacy. Two impact velocities are compared, 4000 and 7000 ft/sec, and 100 replications of the simulation model are performed for each scenario. The impact conditions for these two scenarios are summarized in Table 4. The outputs of interest in this analysis are *N*, the total number of fragments in the debris cloud as determined by Eq. (3), and the average diameters of the debris fragments.

Table 4 Impact Conditions for the Two Scenarios

Scenario	*Target Material*	*Target Thickness (in)*	*Impactor Mass (grains)*	*Impact Velocity (ft/sec)*	*Replications*
1	2024	0.16	75	**4000**	100
2	2024	0.16	75	**7000**	100

Table 5 provides a summary of the output from BISM. Clearly, the higher impact velocity results in a significantly larger number of debris fragments, with a sample mean of 242.3 total fragments (compared to a sample mean of 47.48 fragments for the lower impact velocity). However, an impact velocity of 4000 ft/sec results in larger sized fragments on average, per Eq. (13). For this impact velocity, the average diameter of the impactor spall, $d_{a,s}$, is approximately 2.4 mm and the average diameter of the panel fragments, $d_{a,p}$, is approximately 3.6 mm. On average, the residual impactor's diameter, d_{ri}, is 8.3 mm (see Table 5). For an impact velocity of 7000 ft/sec, $d_{a,s}$ is about 1.6 mm and $d_{a,p}$ is about 2.4 mm. On average, d_{ri} is 6.5 mm (see Table 5). These results generally match the findings discussed in Yatteau and Dickinson (1993). There, micro-crystalline wax was used to collect debris fragments from the impact of hardened steel spheres on mild steel targets at two velocities: 1600 m/sec (5250 ft/sec) and 2400 m/sec (7875 ft/sec). The provided photographs of the collected debris indicate a much larger quantity of fragments (that are considerably smaller on average) for the 7875 ft/sec impact velocity. However, actual fragment sizes are not indicated.

Table 5 BISM Output for the Two Impact Velocities

Output Statistic	*Impact Velocity (ft/sec)*	*Mean*	*Min*	*Max*	*95% CI Half-Width*
N	4000	47.48	11	92	4.0237
	7000	242.3	95	358	10.5083
d_{ri} (mm)	4000	8.295	3.280	8.523	0.1325
	7000	6.476	1.748	8.523	0.3275
$d_{a,s}$ (mm)	4000	2.356	-	-	-
	7000	1.622	-	-	-
$d_{a,p}$ (mm)	4000	3.552	-	-	-
	7000	2.446	-	-	-

Figures 5 and 6 provide screenshots of the animation from a BISM run at the 7000 ft/sec impact velocity. At 0.10 milliseconds after impact, note how the minimal dispersion of the fragments along the y-axis contrasts sharply with the expansion of the cloud along the z-axis. This behavior matches observations made in Kipp *et al* (1993) for actual debris clouds generated from the high-velocity impact of steel spheres on PMMA plastic plates. The general curvature of the debris cloud in Figs. 5 and 6 also resembles radiographic images of actual clouds provided in Yatteau and Dickinson (1993). These screenshots of the simulation model animation, combined with the output provided in Table 5, appear to adequately display the general characteristic behavior of a debris cloud generated by a ballistic impact event. However, it is important to note that results depend heavily on the notional values for the fit variables in the fragmentation model (f_ε, α, β, and τ_f) and must be taken at face value.

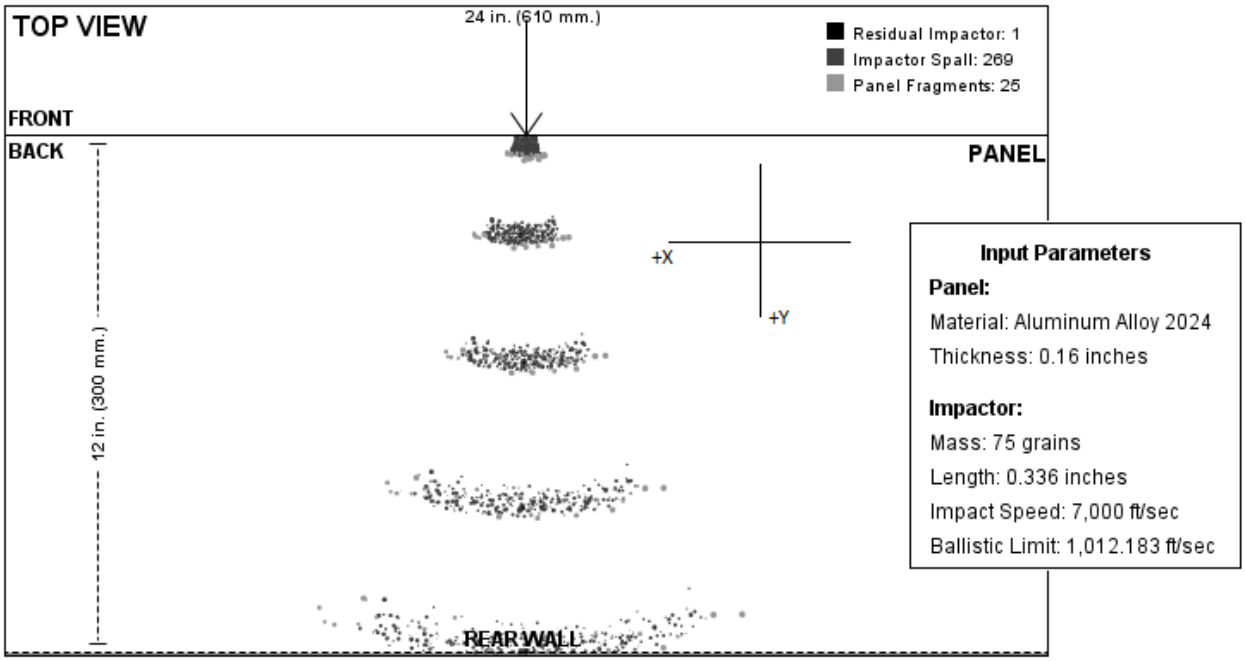

Figure 5 A screenshot of the 2D "top view" animation window during a simulation run.

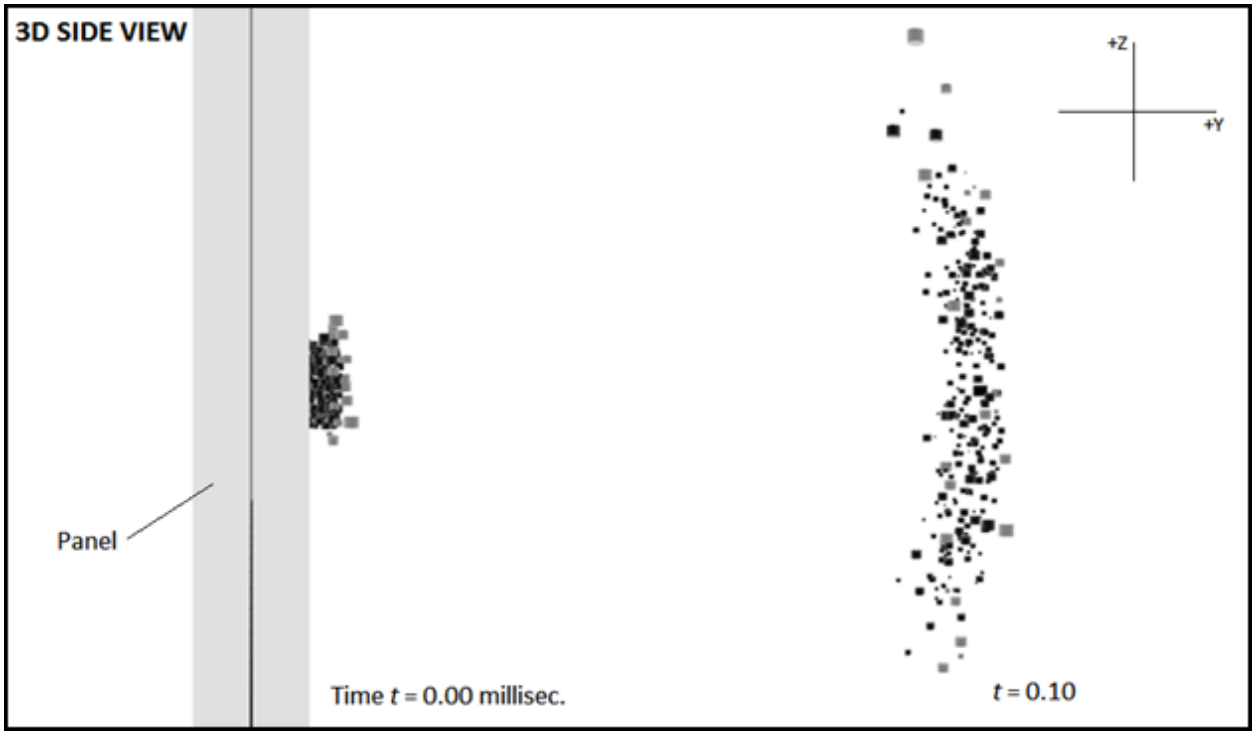

Figure 6 A screenshot of the 3D "side view" animation window during the same simulation run illustrated in Fig. 5.

Focus of Future Work

With an impact fragmentation model incorporated into the current BISM prototype, future work will focus on the development of a model for the thermal profile of a ballistic impact event. A possible avenue for this task utilizes the agent-based approach to modeling debris fragments already in BISM. With such an approach, one can treat each fragment in the debris cloud as a discrete (though not autonomous) "lump" of uniform temperature. By assigning each fragment an initial temperature and giving it a cooling rate dependent on the temperature of its surroundings (that updates as the debris cloud evolves), the heat released by the cloud as a whole can emerge from the simple lower level interactions of the individual agents.

To investigate the feasibility of this concept, we have developed a notional, proof-of-concept thermal model utilizing the following cooling rate for each fragment (based upon Newton's Law of Cooling):

$$\frac{dT_{ft}}{dt} = -r_f\left(T_{ft} - T_{surr,ft}\right), \tag{18}$$

where T_{ft} is the temperature of fragment f at time t, $T_{surr,\,ft}$ is the temperature of the surroundings of f at time t, and r_f is a cooling coefficient dependent on the material properties of f. Eq. (18) is incorporated into the model logic shown in Figure 7 for updating $T_{surr,\,ft}$. At time zero in the simulation, each fragment computes its initial location within the debris cloud. Fragments with initial locations on the outer edge of the cloud are assumed to be exposed to the ambient "room" temperature of the surroundings (approximately 295 K). For these fragments T_{surr} is set to room temperature for the entire simulation run. Fragments in the interior of the cloud update their value of T_{surr} at each time step by computing the distance-weighted average temperature of neighboring fragments. These rules for computing surrounding temperatures drive the overall cooling of the debris cloud, resulting in an "outside-in" cooling phenomenon.

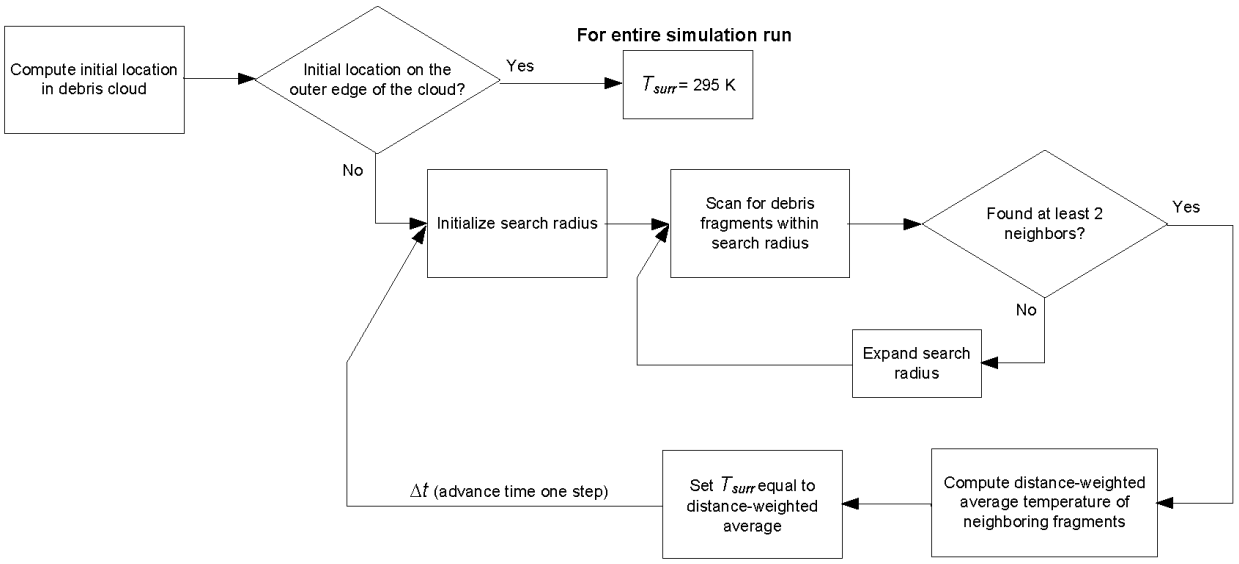

Figure 7 Flowchart logic for updating the surrounding temperature, T_{surr}, of each fragment.

Initial comparisons of the model to experimental data from Buck *et al* (2011) appear promising. Figure 8 provides side-by-side plots of a temperature time series for test shot T050 (mild steel impacting BMI composite at unknown velocity) and results from a BISM run (75 grain mild steel impacting 0.09 inch aluminum 2024 at 5,500 ft/sec). While the initial peak temperature used in the simulation is notional, both time series exhibit roughly the same rise and decay pattern. In each plot, it takes approximately 2 milliseconds for the cloud temperature to drop from its peak level to below 500 K. These initial results suggest that this approach, while highly simplistic, has the potential to reasonably model the complex thermal behavior of a ballistic impact event without diving into the more detailed physics involved. As more experimental data becomes available, an empirical approach combined with the consultation of heat transfer experts can yield a more realistic model.

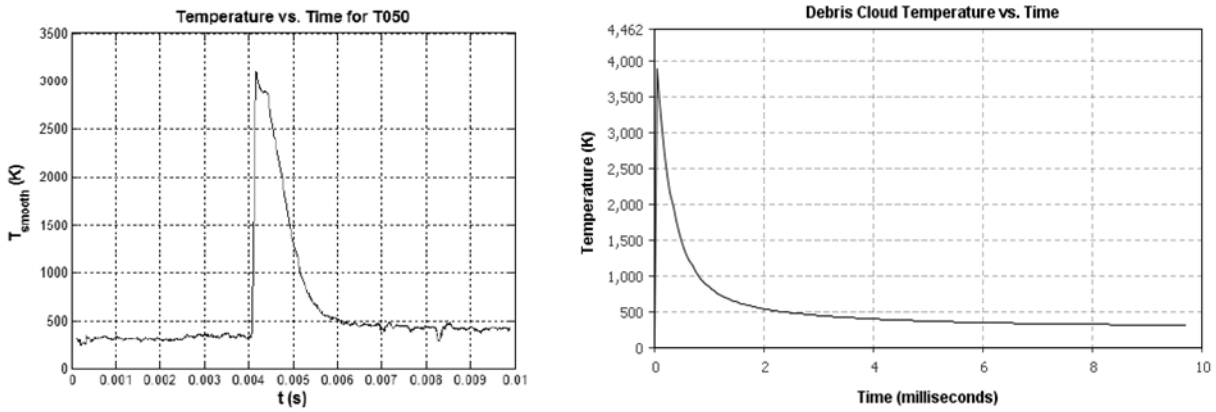

Figure 8 (Left) temperature time series for test shot T050 from Buck *et al* (2011), time of impact = 4 milliseconds; (right) temperature time series obtained from a BISM run, time of impact = 0 milliseconds.

Concluding Remarks

This paper presents a proof-of-concept, agent-based simulation model of the complete secondary threat resulting from a ballistic impact event. An impact fragmentation model specifying the quantity, size distribution, and initial state of motion of the fragments in the debris cloud has been developed and incorporated into the BISM prototype. Validation of this model and extension to other impact conditions awaits necessary experimental data. The focus of future work, an agent-based thermal model of a ballistic impact event, has been proposed and notionally developed.

Initial evaluations of the simulation model appear promising and suggest that further development is worthwhile. Future iterations of BISM, combined with fire prediction codes, can prove to be valuable in vulnerability assessments of military vehicles. Depending on the needs of the end user, a fire prediction module can even be developed for incorporation into BISM, involving the interaction of heated debris fragments and fuel spurt components from a punctured fuel bladder (another class of agents). However, there is a limit to such extensions, as each layer of added complexity dramatically increases run times in continuous simulation models.

Aircraft survivability focuses on mitigating onboard fires caused by external threats, such as impacting missile fragments. These projectiles, upon penetrating the aircraft, can impact fuel bladders and cause potentially hazardous fires. No analytical models exist to examine such

situations. Our BISM provides a crucial first component for an eventual analytical approach to help improve aircraft survivability.

Acknowledgements

Matthew Bova was supported by the Southwestern Council for Higher Education (SOCHE) and Dr. Frank Ciarallo by the Oak Ridge Institute for Science and Education (ORISE). The research was funded under the Science of Test Research Consortium within the Air Force Institute of Technology, Center for Operational Analyses. The authors would like thank Mr. Scott Wacker and the US Air Force Aerospace Survivability and Safety Operating Location (96 TG/OL-AC) at Wright-Patterson Air Force Base for providing the experimental data used in model development and the required subject matter expertise.

Disclaimer: The views expressed in this article are those of the author and do not reflect the official policy or position of the United States Air Force, Department of Defense, or the US Government.

References

Bestard JJ and Kocher B (2010). Ballistic impact flash characterization. *51st AIAA/ASME/ASCE/AHS/ASC Structures, Structural Dynamics, and Materials Conference*. American Institute of Aeronautics and Astronautics: Orlando, FL, 12–15 April.

Bjorkman MD, Geiger JD, and Wilhelm EE (1987). *Space station integrated wall design and penetration damage control, task 3: theoretical analysis of penetration mechanics*. Final report, Contract no. NAS8-36426. Seattle, WA: Boeing Aerospace Corporation.

Bova M, Ciarallo FW, and Hill R (2013). A prototype model of fire ignition from ballistic impacts. In: Krishnamurthy A and Chan WKV (eds). *Proceedings of the 2013 Industrial and Systems Engineering Research Conference*. Institute of Industrial Engineers: San Juan, PR, pp 2084–2091.

Buck MD, Kocher BD, and Bestard JJ (2011). Thermal profile measurements for ballistic impact flashes. *52nd AIAA/ASME/ASCE/AHS/ASC Structures, Structural Dynamics, and Materials Conference*. American Institute of Aeronautics and Astronautics: Denver, CO, 4–7 April.

Grady DE and Kipp ME (1985). Geometric statistics and dynamic fragmentation. *Journal of Applied Physics* **58**(3): 1210–1222.

Grady DE and Winfree NA (2001). Impact fragmentation of high-velocity compact projectiles on thin plates: a physical and statistical characterization of fragment debris. *International Journal of Impact Engineering* **26**: 249–262.

Greer R and Hatz M (1992). *KAPP-II user's manual, version 1.1*. Report, K92-17U(R). Colorado Springs, CO: Kaman Sciences Corporation.

Heath BL and Hill RR (2010). Some insights into the emergence of agent-based modeling. *Journal of Simulation* **4**(3): 163-169.

Joint Technical Coordinating Group for Munitions Effectiveness (1985). *Penetration equations handbook for kinetic-energy penetrators*. Report, 61 JTCG/ME-77-16. Washington, DC: US Department of Defense.

Kipp ME, Grady DE, and Swegle JW (1993). Numerical and experimental studies of high-velocity impact fragmentation. *International Journal of Impact Engineering* **14**: 427–438.

O'Connell PJ, Brickson ET, Miller ML, and Cyphers DC (2010). *Panel testing of materials representative of large commercial aircraft: detailed test plan*. Report, Wright-Patterson AFB: 96 TG/OL-AC.

Pyles JM and Disimile PJ (2011). Thermal model for ballistic impact flashes. *52nd AIAA/ASME/ASCE/AHS/ASC Structures, Structural Dynamics, and Materials Conference*. American Institute of Aeronautics and Astronautics: Denver, CO, 4–7 April.

Schäfer FK (2006). An engineering fragmentation model for the impact of spherical projectiles on thin metallic plates. *International Journal of Impact Engineering* **33**: 745–762.

Schonberg WP (1995). A comparison of fragmentation models. *International Journal of Impact Engineering* **17**: 739–750.

Snow P (1992). *KAPP—Kaman analytical penetration program*. Report, K85-7U(R). Colorado Springs, CO: Kaman Sciences Corporation.

Talafuse T, Hill RR, and Bestard JJ (2011). Characterization of ballistic impact flashes – empirical model development. *52nd AIAA/ASME/ASCE/AHS/ASC Structures, Structural Dynamics, and Materials Conference*. American Institute of Aeronautics and Astronautics: Denver, CO, 4–7 April.

Yatteau JD (1982). *High velocity multiple plate penetration model*. Report, NSWC TR 82-123. Denver, CO: Denver Research Institute.

Yatteau JD and Dickinson DL (1993). An engineering model to predict perforation damage to plates impacted by high velocity debris clouds. *International Journal of Impact Engineering* **14**: 831–842.

Matthew J. Bova is an undergraduate student at the University of Cincinnati and a SOCHE summer intern at the Air Force Institute of Technology. He is pursuing dual degrees in Statistics and Economics, with a minor in Operations Research. Upon completion of his undergraduate studies in April 2014, he plans to pursue advanced degrees in Operations Research. His email address is bova.matthew@gmail.com.

Frank W. Ciarallo is an Associate Professor in the College of Engineering & Computer Science at Wright State University. He has a Ph.D. in Industrial Administration and a B.S. in Electrical & Computer Engineering, both from Carnegie Mellon University. His research interests include simulation modeling architectures, applications of simulation, modeling uncertainty and risk in supply chains and multiobjectivization in genetic algorithms. He is a member of the Institute for Operations Research and the Management Sciences (INFORMS), the Institute of Industrial Engineers (IIE) and the Institute of Electrical and Electronic Engineers (IEEE). His email address is frank.ciarallo@wright.edu.

Raymond R. Hill is a Professor of Operations Research with the Air Force Institute of Technology. He has a Ph.D. in Industrial and Systems Engineering from The Ohio State

University. His research interests include applications of simulation, applied statistical modeling, mathematical modeling, decision analytical methods, the design and analysis of heuristic optimization methods, and agent-based modeling. He is a member of the INFORMS, the Military Applications Society of INFORMS, the Military Operations Research Society (MORS), the International Test and Evaluation Association, and the Institute of Industrial Engineering (IIE) and is a former Director of the Operations Research Division of the IIE. He is an Associate Editor for Naval Research Logistics, Military Operations Research, the Journal of Defense Modeling and Simulation, and the Journal of Simulation. He was a proceedings co-chair for both the 2008 and 2009 Winter Simulation Conferences and will serve as the General Chair for the 2013 conference. His email address is rayrhill@gmail.com.